An Assessment of Non-geophysical Effects in Spaceborne GNSS Reflectometry Data From the UK TechDemoSat-1 Mission

Giuseppe Foti, Christine Gommenginger, Martin Unwin, Philip Jales, Jason Tye, and Josep Roselló

***Abstract*—An assessment of non-geophysical effects in spaceborne global navigation satellite system reflectometry (GNSS-R) data from the UK TechDemoSat-1 (TDS-1) mission is presented. TDS-1 was launched in July 2014 and provides the first new spaceborne GNSS-R data since the pioneering UK-disaster monitoring constellation experiment in 2003. Non-geophysical factors evaluated include ambient L-band noise, instrument operating mode, and platform-related parameters. The findings are particularly relevant to users of uncalibrated GNSS-R signals for the retrieval of geophysical properties of the Earth surface. Substantial attitude adjustments of the TDS-1 platform are occasionally found to occur that introduce large uncertainties in parts of the TDS-1 GNSS-R dataset, particularly for specular points located outside the main beam of the nadir antenna where even small attitude errors can lead to large inaccuracies in the geophysical inversion. Out of eclipse however, attitude adjustments typically remain smaller than 1.5°, with larger deviations of up to 10° affecting less than 5% of the overall sun-lit data. Global maps of L1 ambient noise are presented for both automatic and programmed gain modes of the receiver, revealing persistent L-band noise hotspots along the Equator that can reach up to 2.5 dB, most likely associated with surface reflection of signals from other GNSS transmitters and constellations. Sporadic high-power noise events observed in certain regions point to sources of human origin. Relevant conclusions of this study are that platform attitude knowledge is essential and that radiometric calibration of GNSS-R signals should be used whenever possible. Care should be taken when considering using noise measurements over the equatorial oceans for calibration purposes, as ambient noise and correlated noise in delay–Doppler maps both show more variation than might be expected over these regions.**

***Index Terms*—Ambient noise, attitude control, global navigation satellite system (GNSS), GNSS reflectometry (GNSS-R), GNSS remote sensing, ocean remote sensing, radiofrequency interference (RFI), spaceborne radar, TechDemoSat-1 (TDS-1).**

Manuscript received September 15, 2016; revised December 23, 2016; accepted January 26, 2017. Date of publication May 30, 2017; date of current version July 26, 2017. This work was supported in part by the European Space Agency and in part by the Natural Environment Research Council. *(Corresponding author: Giuseppe Foti.)*

G. Foti and C. Gommenginger are with the National Oceanography Centre, Southampton SO143ZH, U.K. (e-mail: g.foti@noc.ac.uk; cg1@noc.ac.uk).

M. Unwin and P. Jales are with Surrey Satellite Technology Limited, Guildford GU27YE, U.K. (e-mail: m.unwin@sstl.co.uk; p.jales@sstl.co.uk).

J. Tye is with the University of Surrey, Guildford GU27XH, U.K. (e-mail: j.tye@surrey.ac.uk).

J. Roselló is with the European Space Agency, European Space Research and Technology Centre, Noordwijk 2201AZ, The Netherlands (e-mail: josep.rosello@esa.int).

Color versions of one or more of the figures in this paper are available online at http://ieeexplore.ieee.org.

Digital Object Identifier 10.1109/JSTARS.2017.2674305

I. Introduction

GLOBAL navigation satellite system reflectometry (GNSS-R) is now a well-known new remote sensing technique exploiting global navigation satellite system (GNSS) signals reflected off the surface of the Earth in a forward scattered bistatic radar configuration, where the transmitter is a GNSS satellite in medium Earth orbit (MEO) and the receiver is a passive instrument on a separate platform such as a low Earth orbit satellite. The use of passive receiving hardware enables the design of low mass, low-power, low-cost instruments that can be flown on constellations of small satellites [1]–[3] or as payloads of opportunity on other platforms/missions. This potential for low-cost implementation provides the option to build a comparably affordable Earth observation system characterized by sensors on multiple satellites to achieve very high spatio-temporal sampling of surface geophysical parameters such as ocean surface winds.

The TechDemoSat-1 (TDS-1) mission is a UK-funded technology demonstration mission that was launched in July 2014 [4]–[6]. Among its eight experimental payloads, it includes the SGR-ReSI, a low mass, low-power, low-cost GNSS reflectometry receiver developed by Surrey Satellite Technology Limited. The SGR-ReSI is a precursor of the GNSS-R receivers to be flown on the NASA CYGNSS mission due for launch in late 2016 [7].

The aim of this paper is to investigate non-geophysical effects on spaceborne GNSS-R signals based on the experience and GNSS-R data acquired with TDS-1. Non-geophysical effects include ambient L-band noise, instrument operations, and platform-related parameters. The analyses focus on the impact of these effects on GNSS-R delay–Doppler maps (DDM) and derived observables of reflected signal power (such as the signal-to-noise ratio, SNR), which are frequently used to relate GNSS-R signals to ocean surface geophysical properties [4], [7], [8].

The paper is organized as follows: Section II presents an overview of the TDS-1 mission, the SGR-ReSI instrument, its operation modes, the different mission phases, and data collected to date. Section III focuses on the observed attitude and noise measurements, Section IV discusses results, and Section V presents the conclusion.

II. TechDemoSat-1 and the SGR-ReSI GNSS-R Receiver

The TDS-1 mission was launched in July 2014 and successfully completed its platform and instrument commissioning

phase in March 2015. Since then, the satellite has been operating nominally throughout its exploitation phase, which will last up to the mission end-of-life expected no sooner than mid-2017. The platform flies at an altitude of 635 km, in a retrograde quasi sun-synchronous orbit with an inclination of 98.4°. The local time of the ascending node at the start of the mission was 21:00, with a constant drift of ∼1.42 h/year. The spacecraft is, therefore, operating under sunlit conditions for descending tracks, while ascending tracks correspond to the spacecraft operating mainly in eclipse. Full details about the mission and the GNSS-R payload can be found in [5] and [6].

The SGR-ReSI receiver, also known as the sea state payload, was designed to demonstrate the suitability of GNSS-R for sea state monitoring applications. The instrument is one of the eight experimental payloads that have to share the platform resources of this low-budget UK technology demonstration mission. For this reason, each payload is allocated specific days on a strict 8-day operating cycle. So far, operation of the GNSS-R payload has been limited to days 1 and 2 for routine data logging and days 7 and 8 for special operations, such as code uploads and experimentation.

The SGR-ReSI receiver can operate in two modes, unmonitored automatic gain control mode (AGM) or programmed gain mode (PGM). The SGR-ReSI instrument was operated continually in AGM from early mission operations until April 2015, then in PGM since May 2015. Fig. 1 shows the volume of data collected in the two operation modes in different phases of the mission and the spatial distribution and coverage of the TDS-1 GNSS-R dataset to date. Overall, the dataset collected between September 2014 and February 2016 represents a total of approximately 22 million 1-Hz DDM of correlated GNSS forward-scattered power (5.8M samples in AGM, 16.3M samples in PGM).

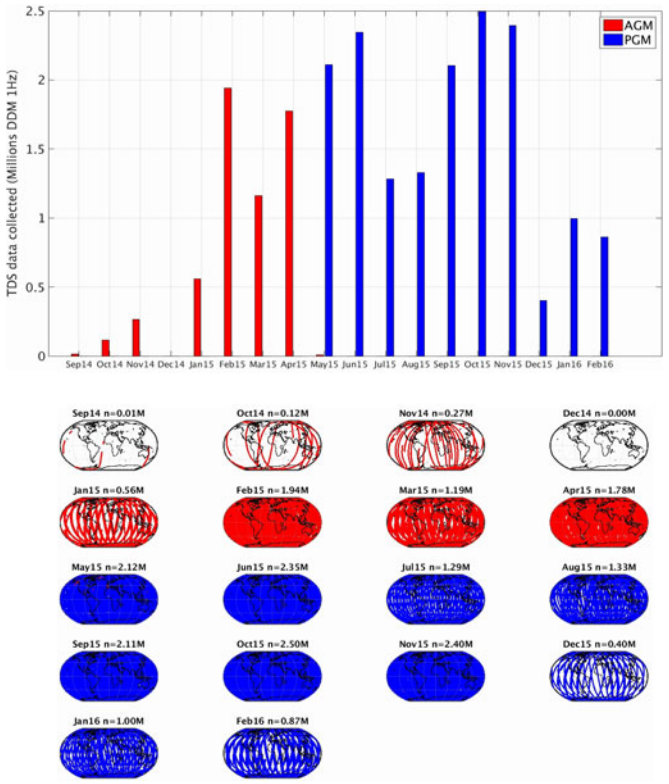

Fig. 1. TDS-1 SGR-ReSI data collected each month between September 2014 and February 2016 showing (top) number of onboard collected 1 Hz DDM and (bottom) spatial distribution and coverage. Shown in red are TDS-1 data acquired in automatic gain mode (AGM), and in blue, TDS-1 data acquired in programmed gain mode (PGM).

A. AGM and PGM

In AGM, the gain of the intermediate-frequency voltage amplifier of the GNSS receiver is adaptively adjusted by the automatic gain control (AGC) according to the incoming power level. The goal of the AGC is to keep the power at the input of the integrated 2-bit analog-to-digital converter (ADC) around an optimal level, to achieve minimum degradation of the signals by the quantization process. The AGC dynamically attempts to adjust the system gain in 1 dB steps to achieve an optimal magnitude bit distribution (MBD) of 33%, which corresponds to minimum implementation loss for the receiver 2-bit ADC. The use of an unmonitored AGC is standard for many GNSS receivers. The MBD expressed as a percentage is a standard output of the instrument that is commonly used to assess receiver performance.

AGM makes it possible for the receiver to deal with a wide range of incoming power levels that can change rapidly and significantly depending on incoming radiation from natural and artificial L-band sources. The AGC mode, thus, offers the advantage of reducing the sensitivity of the system to ambient noise. However, as the AGC operation of the GNSS-R receiver on TDS-1 is unmonitored, the variable gain level is not recorded and it is not possible to recover the information about the absolute level of incoming radiation. Interpretation of the signals, thus, becomes more complex as the operation of the AGC can mask changes in power levels such as those linked to varying antenna noise temperature and/or system noise figure. This introduces additional complexity for the definition of the geophysical model function developed to relate the correlated signal power reported by the instrument to ocean surface conditions.

The SGR-ReSI can also operate in a PGM. When the instrument operates in PGM, the AGC is not active, the gain is set to a known level, and the MBD is directly linked to the integrated noise power incident on the nadir antenna (first-order), with residual effects related to system gain and noise figure, both depending on physical temperature. In April 2015, after 8 months of data acquisition in AGM, a series of in-orbit tests were carried out over 1.5 orbits (∼145 min) to determine the optimum gain level that minimizes quantization losses. In this experiment, the receiver gain was swept through a range of digital values (roughly in 1 dB steps) in order to find the optimal system gain that achieves the optimal MBD of 33%. The value of the optimal gain setting for the MAX2769 GNSS receiver onboard TDS-1 was found to be equal to 36 (gain value programmed in steps of 1 dB). This value represents the optimal setting for this particular period of the mission, but it should be noted that the optimal setting could change slowly in time due to the ageing of the system, the drift in the TDS-1 orbit, and

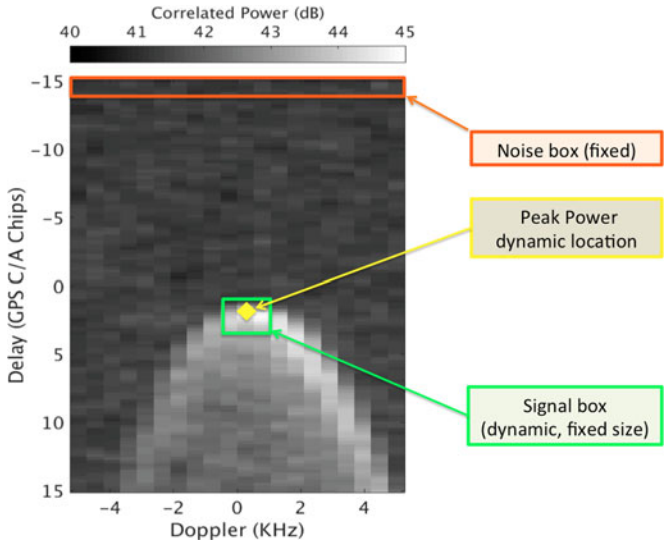

Fig. 2. Example of a delay–Doppler map (DDM) from TDS-1 acquired over the ocean, showing the DDM areas that can be used to estimate the noise power (orange box) and the signal power (green box) positioned dynamically around the peak power (shown in yellow).

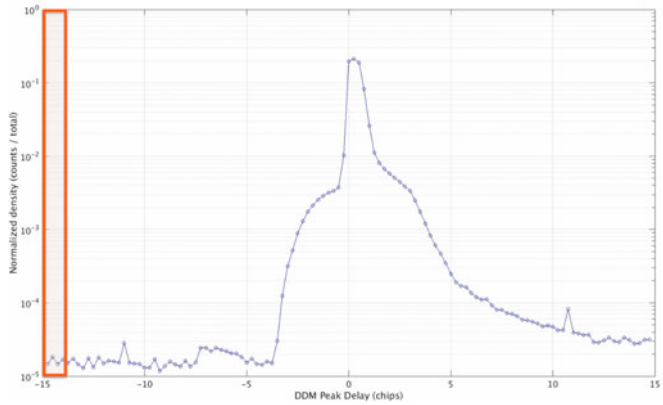

Fig. 3. Distribution of the relative delay of the DDM peak in TDS-1 1 Hz DDM acquired over ocean between September 2014 and February 2016, showing that the noise box adopted (orange) is generally free of reflected signals.

possible variations of on-board physical temperature associated with this. Following this experiment, the SGR-ReSI was reprogrammed to operate routinely with this known gain level of 36 and to collect GNSS-R data in PGM since May 2015.

B. Delay–Doppler Maps, Noise Power, and Signal Power

In GNSS-R ocean remote sensing, the quantity of interest for the retrieval of surface geophysical parameters is the GNSS satellite signal power incident on the receiver antenna after correlation with the pseudo-random noise (PRN) code specific to that satellite. In effect, the received signal has a matched filter applied specific to the target PRN. This signal power measurement is generally extracted from the DDM products, which represent the distribution in delay and Doppler frequency of the GNSS correlated power of a particular PRN code [9]. In order to achieve the necessary spatial resolution, geophysical retrieval of ocean winds has mainly focused on the power level at or around the peak of the DDM, which is related to the forward-scattering by the surface at the specular point (SP). The DDM observable typically chosen to relate to ocean surface winds is the SNR or, less commonly so far, the signal-minus-noise (SMN).

Fig. 2 shows an example of a DDM collected over the ocean by TDS-1 and the areas of the DDM that can be used to estimate the signal and noise power. In this example, based on the work by Foti *et al*. [4], the signal (S) is estimated as the average value in the fixed-sized box shown in green that is positioned dynamically around the peak, while the noise power (N) is estimated as the average value in the fixed-sized box shown in orange, positioned at a fixed location in the first few delay rows of the DDM. The SNR can then be estimated, either as the ratio of S over N, i.e., SNR $= S/N$ or sometimes as SNR $= (S - N)/N = (S/N) - 1$ to account for the thermal noise floor level. Other observables, such as the SMN, can similarly be estimated as SMN $= S - N$. In all cases, the operations are applied to S and N in their linear forms, before typically expressing the resulting observable in dB.

C. Noise Power

Fig. 3 highlights the importance of ensuring that the noise box is positioned well away from the signal peak. For TDS-1, it can be seen that the delay window is very wide (15 chips is equivalent to 4.4 km) and that the peak is located close to the nominal tracking point (at 0 chips). Over the ocean, the nominal tracking point corresponds to the predicted delay of the peak assuming the SP is located on the reference ellipsoid. Departures of the peak position from this nominal tracking point are related to ranging differences introduced by the ionosphere, changes in sea surface height above the ellipsoid, and residual uncertainties linked to positioning and navigation. Fig. 3 shows the distribution of the position in delay space of the DDM peak signal for TDS-1 1 Hz DDM acquired over ocean between September 2014 and February 2016. The results clearly indicate that, for TDS-1, the signal peak typically occurs at delays greater than –5 chips, so that that the power estimated in the first few delay bins (the noise box) is usually uncontaminated by autocorrelated GNSS signal power. In the few rare cases when the maximum power of the waveform is found in the noise box, these have been linked to radiofrequency interference (RFI) events.

In AGM, the noise is continually normalized, but when in PGM, the noise power represents a measure of the antenna noise temperature. This can be measured in two ways—one is through the MBD prior to correlation, available from the instrument telemetry, and the other is from noise regions of the DDM, after correlation with the target PRN. The antenna noise temperature is the integration of all incident L-band radiation in the antenna field-of-view (FOV). Sources of ambient L-band noise include natural background radiation (cosmic, Galaxy, Sun, Moon, etc.), but also contributions from man-made transmitters at L-band. Artificial ambient noise components might comprise L-band radiation originating from space or reflected off the surface of the Earth (e.g., other GNSS satellites including some in geostationary orbits) or directly from surface-based emitters (GNSS beacons, pseudolites, jammers, etc.).

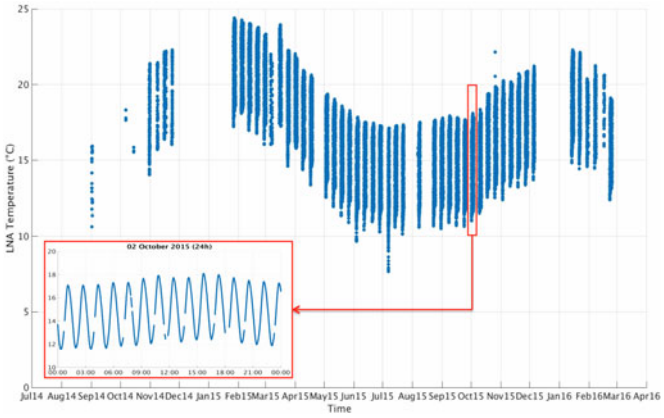

Fig. 4. Long-term evolution of SGR-ReSI low noise amplifier (LNA) temperature on-board TechDemoSat-1 between September 2014 and February 2016, and variability over 24 h (inset).

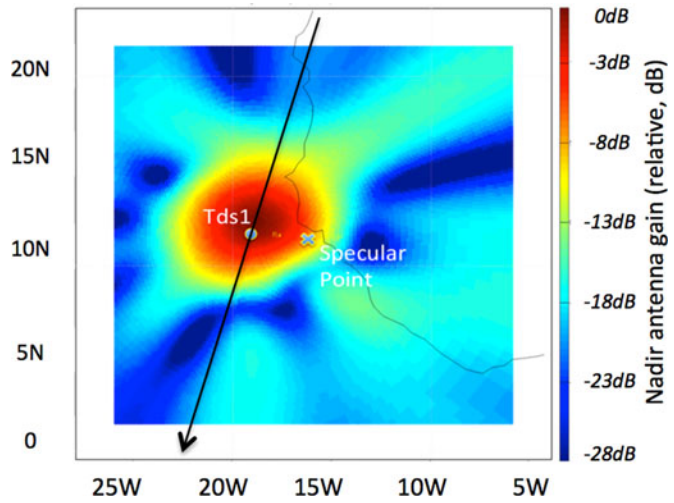

Fig. 5. TDS-1 SGR-ReSI nadir antenna normalized gain map projected on the Earth surface assuming nominal platform attitude, with the black arrow representing the TDS-1 descending track. This example is shown for a location west of Senegal in West Africa.

D. Signal Power

In the case of the signal power, as well as being related to the scattering geometry and the surface geophysical properties of interest (e.g., [10], [11]), the signal power is also sensitive to a number of non-geophysical factors related to the specifics of the receiving apparatus. In particular, with reference to the SGR-ReSI receiver on TDS-1, the main parameters affecting the signal power are the antenna gain at the SP (AGSP), the system noise figure, quantization losses, and system gain. The effect of these can be estimated through absolute calibration. However, although the SGR-ReSI has the capability to perform radiometric calibration on-board, this facility has only recently started to be exploited and analyses are still underway. Hence, all scientific investigations with TDS-1 GNSS-R have so far been limited to uncalibrated signals.

Taking these non-geophysical effects on signal power in turn, the AGSP is found to be a first-order effect on the strength of the PRN-matched signal originating from the glistening zone around the SP. Accurate knowledge of the AGSP is, therefore, of primordial importance for geophysical retrieval, and this is explored in more detail in the next section.

The system noise figure is essentially driven by the noise figure of the low noise amplifier (LNA) in the front-end. For TDS-1, the LNA noise figure variation is relatively small, as the nominal figure ($\sim$2.7 dB) changes with temperature only by about 0.01 dB per degree centigrade. Fig. 4 shows the long-term evolution of the on-board LNA temperature, which fluctuates within a range of around 15°C between September 2014 and February 2016. Variability along the orbit (shown in Fig. 4 inset as the evolution over 24 h) is typically of the order of 5°C. This corresponds to a noise figure variation of less than 0.1 dB, which can be neglected for the retrieval. As seen in the previous section, quantization losses are minimized either through the use of AGM, or by setting the programmed system gain in PGM to a value that minimizes these losses.

Finally, the system gain is defined by the instrument operating mode. As seen above, in AGM, the system gain is an unknown variable, while in PGM, it has a known programmed value. Since the system gain affects both the DDM signal and noise power, it is useful to compute the SNR, which cancels out the effect of the system gain. Using SNR is particularly beneficial in AGM, where it removes the effect of the unknown system gain. In PGM, using the SNR has the same effect, although it merely cancels out the effect of the known system gain. Assuming that system gain and noise figure are sufficiently stable, PGM offers additional strategies for signal estimation, such as the SMN, which offer the potential advantage of reducing the sensitivity of the observable to ambient noise power.

E. Antenna Gain, Platform Attitude, and Eclipse

The SGR-ReSI nadir antenna is a highly directional single-beam high-gain (approximately 13.3 dBi) dual-frequency GPS downwards pointing antenna, with a slight off-pointing of 6° behind the platform away from the direction of flight. The antenna half-power beamwidth (–3 dB) is approximately 30°, while the –6 dB FOV is approximately 45°. As noted above, accurate determination of the AGSP is essential for geophysical exploitation of the signals. With a highly directional antenna, the accuracy with which the AGSP can be determined depends on two elements: good knowledge of the actual antenna gain map and good knowledge of the attitude of the spacecraft.

The SGR-ReSI antenna gain map was characterized on the ground prior to integration with the satellite and has been made available through the TDS-1 MERRByS data portal (MERRByS 2016). The pattern testing took place on a simplified representation of the TDS-1 nadir panel, so some changes are expected to sidelobes due to differences on the real facet. An illustration of the available SGR-ReSI antenna normalized gain map projected on the Earth surface is shown in the bottom right subplot in Fig. 5, assuming nominal platform attitude.

The figure reveals the well-defined antenna main lobe, with high-gain values along the track just behind the satellite and a reasonably isotropic distribution in azimuth for gain values

down to around –6 dB from the peak, but with steep gradients when away from the boresight. At boresight, an unknown attitude off-pointing error of 5° will give an error in gain knowledge of 0.5 dB, while at –6 dB, a 5° offset will give a 3 dB error in gain knowledge. Beyond the main lobe, there is a narrow region of very steep gradients beyond which large irregular peaks-and-troughs in gain occur. Hence, outside the antenna main lobe, the antenna gain presents significant anisotropy in azimuth and rapid changes with incidence.

Platform attitude can be defined relative to a reference system centered on the satellite with positive z-axis pointing toward the center of the Earth, the positive y-axis normal to the (x, z) orbital plane and positive x-axis making up the right-angled set (nominally pointing in the satellite direction of travel). In this coordinate system, the TDS-1 attitude control system aims to maintain a nominal attitude of (0,0,0)° in roll, pitch, and yaw, respectively. The TDS-1 attitude control system is based on an onboard Kalman filter that takes inputs from the onboard magnetometer, sun sensors, and also known actuation commands (wheel spin and magnetorquer firings) and fits the attitude estimate with a model of the satellite attitude dynamics. While the platform is in eclipse of the Earth, the sun-sensor readings are meaningless, and are disregarded. Hence, during the eclipse, the Kalman filter coasts with an under-determined magnetometer-based solution, and attitude uncertainty grows until the sun-sensor measurements are available once more. The TDS-1 attitude knowledge has a baseline accuracy of 2.4° in each axis (3 sigma) in the noneclipsed part of the orbit but there is evidence that it grows to around 10° during eclipse. According to this, one expects the largest attitude uncertainty to occur in the eclipsed part of the orbit and the greatest errors on gain to be seen where the antenna pattern gradient is the highest, away from the boresight.

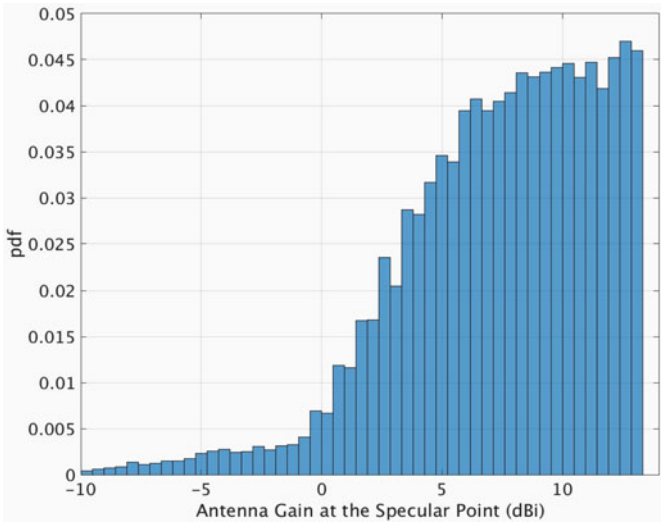

Fig. 6. Probability distribution of TDS-1 antenna gain at the specular point (AGSP in dB) for SP collected over ocean surfaces over the period September 2014–February 2016.

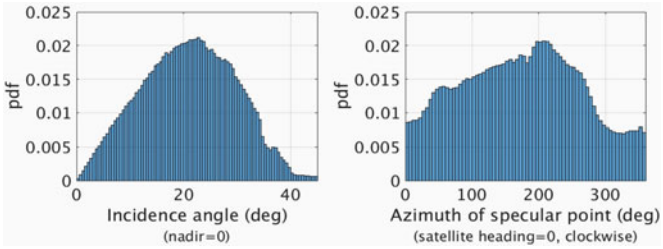

Fig. 7. Probability distribution of TDS-1 specular points (left) incidence angle (right) azimuth angle with respect to satellite body frame of reference. TDS-1 data correspond to the period September 2014–February 2016.

III. Results

A. TDS-1 AGSP and SP Distributions

We start by examining the distributions (PDF) of SPs collected with TDS-1 over all surfaces between September 2014 and February 2016. A system of polar coordinates is adopted to locate the SP with respect to the satellite position and satellite body reference frame, with incidence angles measured from nadir (0°) immediately below the satellite, and SP azimuth angles defined clockwise relative to the front of the spacecraft (azimuth = 0° is immediately ahead of the satellite).

Fig. 6 presents the PDF of the AGSP estimated for TDS-1 data over ocean assuming nominal platform attitude. The PDF comprises only TDS-1 data for which a peak was successfully detected in the DDM. We find that a large proportion (∼60%) of SPs occurs within the –6 dB beam (i.e., AGSP larger than 7.3 dB).

Fig. 7 presents the corresponding PDF of SP incidence and azimuth angles for the same dataset, clearly showing that the distributions are not uniform. Fig. 7 (left) shows the distribution of SP with incidence angle and indicates that the largest number of SP (∼75%) is collected by TDS-1 at incidence angles between 10° and 30° with a peak around 22°. The peak number of samples, thus, occurs for SP close to the –6 dB antenna gain contour (i.e., AGSP ∼7.3 dB), outside the half-power beam of the nadir antenna. The distribution indicates that a non-negligible number of SP (∼40%) is routinely detected outside the main-lobes where the antenna pattern is not known to a high degree of confidence.

Finally, Fig. 7 (right) shows the distribution of SP in azimuth, which reveals a strong anisotropy with, in particular, a much smaller number of SP collected ahead of the satellite, probably linked to the reduced gain in this sector because of the backward pointing of the antenna. Referring to the antenna pattern shown in Fig. 4, this appears to correspond to the anisotropies in the main lobe pattern while the gain is –8 dBi or greater (indicated by orange to red regions), including the noticeable peak at 210°.

B. TDS-1 Eclipse Flag

The TDS-1 level 1 products distributed via MERRByS include the provision of an eclipse flag derived from the onboard sun-sensor measurements, that indicates whether the spacecraft is, or is not, in view of the sun when data from a particular SP are acquired. The eclipse flag is useful for quality control and to reduce the impact of platform attitude uncertainty. Unfortunately, its implementation in early versions (version 0.4 and

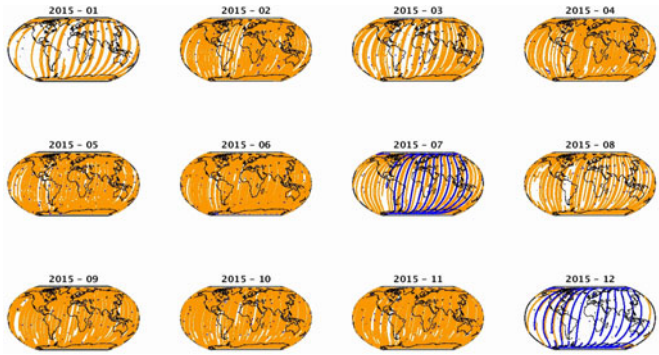

Fig. 8. Monthly maps of the TDS-1 eclipse flag based on onboard sun-sensor data for TDS-1 descending tracks. The figure shows one year of data in 2015. Orange and blue colors indicate sunlit (i.e., out-of-eclipse) and dark (i.e., in-eclipse) conditions.

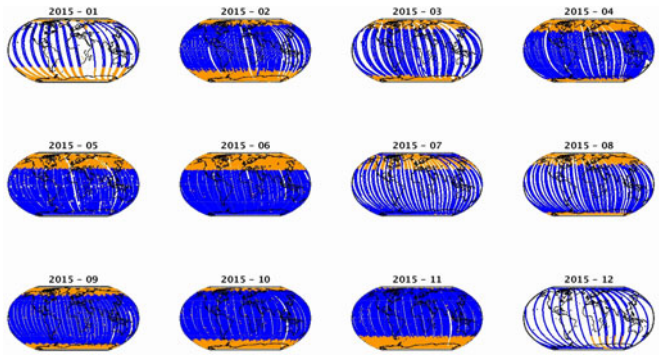

Fig. 9. Monthly maps of the TDS-1 eclipse flag based on onboard sun-sensor data for TDS-1 ascending tracks. The figure shows one year of data in 2015. Orange and blue colors indicate sunlit (i.e., out-of-eclipse) and dark (i.e., in-eclipse) conditions.

earlier) of the TDS-1 level 1 products was incorrect, but with analysis and refinement, the flag was corrected, and the results presented here correspond to the revised eclipse flag data provided in MERRByS L1 data version 0.5 disseminated from May 2016.

Figs. 8 and 9 present global monthly maps of the TDS-1 eclipse flag for descending and ascending tracks, respectively.

For descending tracks, it shows that the sun sensor is generally active at all latitudes, indicating that the spacecraft is within sight of the sun for the full half-orbit. For ascending passes, the eclipse flag indicates that the platform is in eclipse for part of the half-orbit, typically about 72% of the half-orbit, with high-latitude transitions that move latitudinally through the year in accordance with the seasonal cycle. Overall, the revised TDS-1 eclipse flag behaves as expected, except for some minor anomalies, which are currently under investigation (e.g., Fig. 8 July and December 2015; anomalous flagging over small dots at regular interval along the tracks, in both ascending and descending tracks).

C. TDS-1 Platform Attitude Estimates

The onboard attitude determination system is responsible for estimating and maintaining TDS-1 spacecraft in nominal attitude. The Kalman filter attitude estimates are recorded and

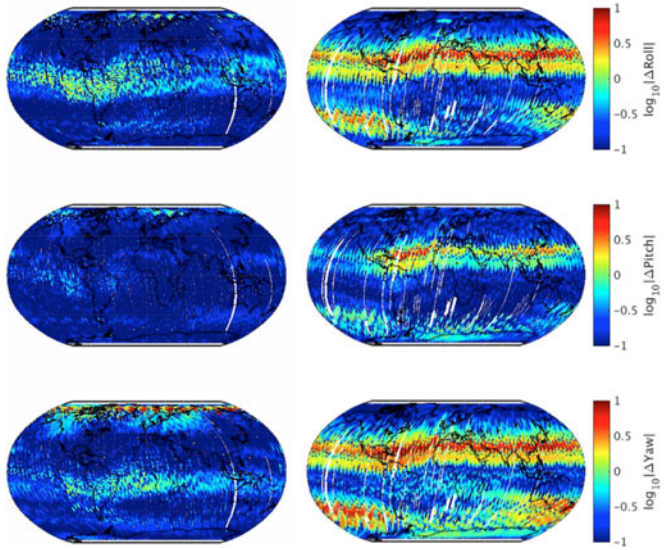

Fig. 10. Geolocated platform attitude estimate (log10, degrees) as reported by the on-board attitude determination system from August 2015 until October 2015. Left column: descending passes (sunlit); right column: ascending passes (part-eclipsed). Different rows show the corrections to platform: (first row) roll, (second row) pitch, and (third row) yaw.

provided with MERRByS. These estimates are based on readings from sensors and fitted on-board with a model of the satellite's attitude dynamics. The sensors provide noisy, biased, and sometimes underdetermined measurements so the attitude estimate will generally be in error by an unknown amount. Any deviations in the estimates from 0° are used by the control system to return the satellite to 0° roll pitch and yaw and imperfect knowledge of actuations and satellite dynamics can introduce lag and overshoot effects.

While this does not represent a direct measurement of the platform attitude, it provides some insight into the circumstances when platform attitude adjustments occur. In particular, discontinuities indicate that a measurement has changed faster than the model anticipated. Fig. 10 presents global maps of the attitude corrections as reported by the TDS-1 onboard attitude determination system for TDS-1 data collected between August 2015 and October 2015. The left column corresponds to data obtained for descending passes (sunlit) while the right column presents the data recorded during ascending passes (part-eclipsed). Absolute deviations from nominal attitude are presented with a log color scale for the roll, pitch, and yaw axes in the first, second, and third rows, respectively.

For ascending passes (part-eclipsed), the reported attitude corrections are generally close to zero in the eclipsed part of the orbit, except for a band of slightly elevated corrections of the order of 1° around the Equator. However, recalling that attitude determination relies solely on the on-board magnetometer during eclipse, the attitude estimate is underdetermined and that the error in the estimate is likely to be growing. This is confirmed by the sudden large attitude adjustments observed as the satellite ascends and exits the eclipsed sector. As the Sun suddenly becomes visible again, the sun-sensor readings are

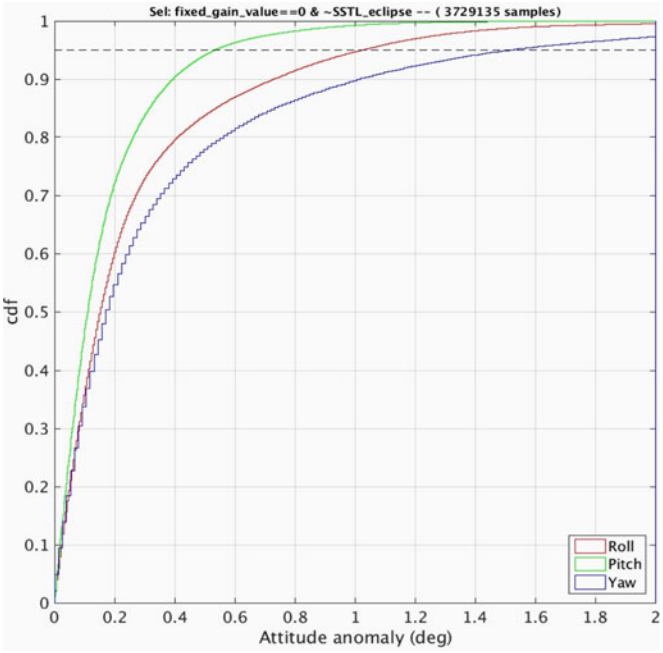

Fig. 11. Cumulative distribution of platform attitude corrections applied during descending passes (sunlit) between September 2014 and April 2015. The attitude corrections are reported by the onboard attitude determination system, showing (red) roll, (green) pitch, and (blue) yaw.

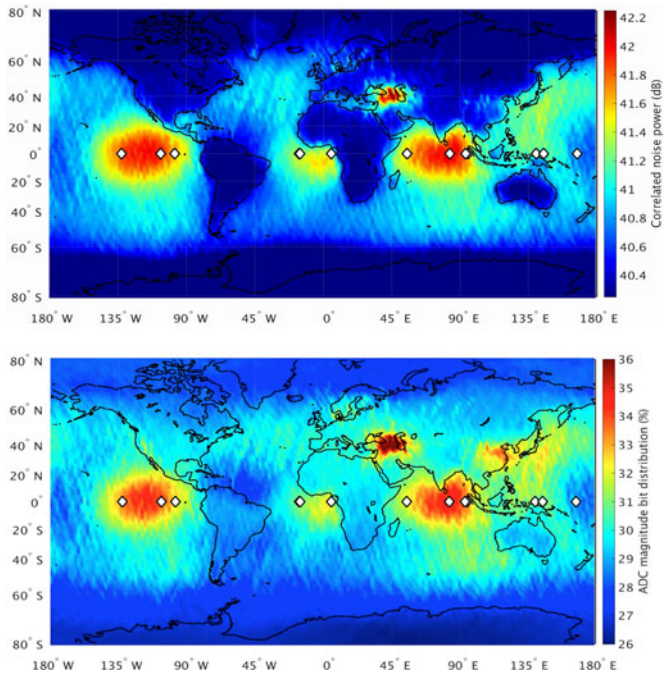

Fig. 12. Mean L1 ambient noise on a 2° × 2° global grid for uncalibrated TDS-1 data acquired in PGM between May 2015 and February 2016 estimated from (top) the DDM-correlated noise power (N) and (bottom) the magnitude bit distribution (MBD) reported by the on-board analogue-to-digital converter. White lozenges indicate the average position of satellite-based augmented system (SBAS) satellites.

incorporated, and it triggers large attitude corrections of the order of 10° in yaw.

For descending passes (sunlit), very large attitude corrections reaching up to 10° in roll, pitch, and yaw are unexpectedly observed in several zonal bands at midlatitudes in both hemispheres. The origin of these large attitude deviations is currently under investigation. Note, however, that these large attitude adjustments affect only a small proportion of the TDS-1 data, as indicated by Fig. 11 which confirms that 95% of the TDS-1 data collected in descending passes (sunlit) during that period corresponds to attitude estimates smaller than 1.5°.

D. L1 Ambient Noise in Spaceborne GNSS-R Data

The SGR-ReSI provides two ways of estimating the ambient noise sensed by the nadir antenna at L1: from the correlated noise power in the DDM (i.e., N, see Fig. 2), and from the MBD reported by the on-board ADC. The two estimates of L1 ambient noise represent related but slightly different measurements: the MBD represents—albeit in a nonlinear way (e.g., [12], [13])—the total L1-band radiation picked up within the TDS-1 antenna beam and detected in the bandwidth of the front-end of the instrument; the DDM-correlated noise power (N) represents the same but measured after PRN correlation by the on-board matched filter.

1) Observed L1 Ambient Noise in PGM: The two estimates of L1 ambient noise are shown in Fig. 12 on a global 2 × 2 degrees interpolated grid for TDS-1 uncalibrated data acquired in PGM between May 2015 and February 2016. The global mean MBD of the instrument when operating in PGM is 29.2% with a range of 12%. This is close to the optimal value of 33%; therefore, indicates that the programmed gain value of $G = 36$ used during that period is appropriately minimizing implementation losses [12].

Fig. 12 confirms that, over the ocean, the DDM-correlated noise power and the MBD show very similar patterns of L1 ambient noise. In fact, both datasets reveal several unexpected and significant L1 radiation hotspots in the Equatorial East Pacific, Indian Ocean, Equatorial Atlantic and, to a lesser extent, the North-Western Pacific. These could be linked to signals from other GNSS transmitters including some in geostationary orbits such as the satellite-based augmented system (SBAS) satellites, whose locations are indicated by white lozenges in Fig. 12. This is explored in more detail below.

Most notable over land are the high-power emissions in the GPS L1 band observed over regions such as Ukraine, the Middle East, East China, and Scandinavia. The intermittency, large power range (not shown), and geo-political context of these emissions point to radio frequency interference of human origin. Further insight into the nature of these sources is gained from looking at the differences in the DDM-correlated noise and MBD maps, whereby only some sources persist in the DDM-correlated noise, making them likely to originate from active GNSS-related systems such as beacons, pseudolites, or jammers.

Elsewhere over ice-free land, the MBD- and the DDM-correlated noise are relatively uniform and show significantly lower ambient noise levels compared to the ocean. The land/ocean contrasts are much greater for DDM-correlated noise

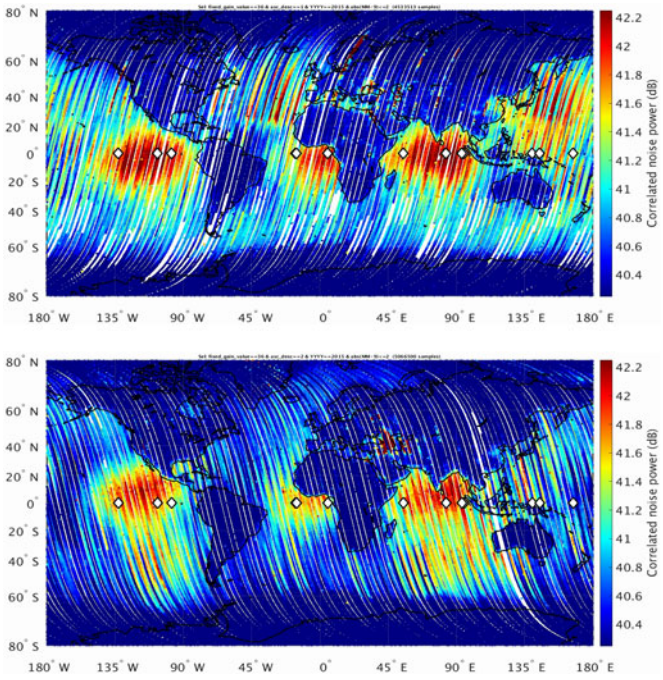

Fig. 13. TDS-1 DDM-correlated noise power (N) for uncalibrated data acquired in programmed gain mode (PGM) between May 2015 and February 2016 for (top) descending tracks (sunlit) and (bottom) ascending tracks (part-eclipsed). White lozenges as in Fig. 12.

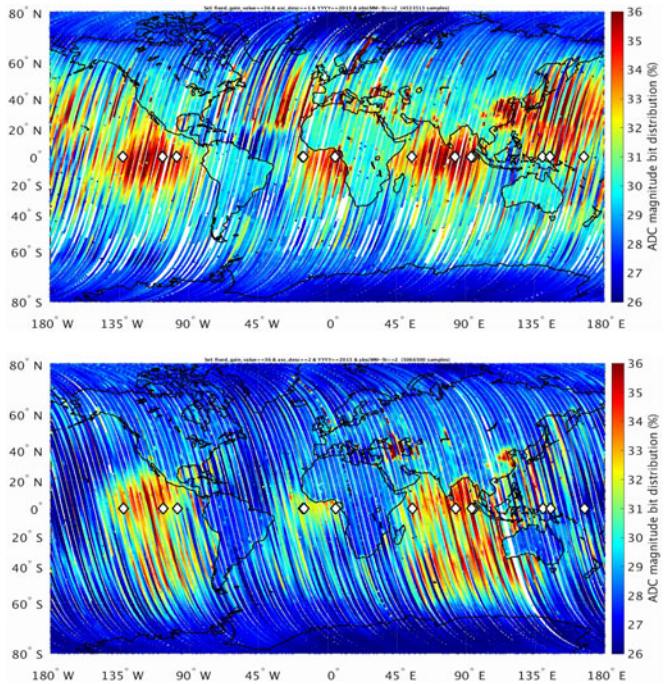

Fig. 14. TDS-1 magnitude bit distribution (MBD) for uncalibrated data acquired in programmed gain mode (PGM) between May 2015 and February 2016 for (top) descending tracks (sunlit) and (bottom) ascending tracks (part-eclipsed). White lozenges as in Fig. 12.

than for MBD. The MBD maps suggest a possible relation between L1 ambient noise and land surface temperature but closer investigation indicates that this relation is spurious (e.g., no relation with surface temperature over the Himalayas; lower MBD over hot South America and central Australia than over hot central Sahara and cool Southern Scandinavia). No relation with land surface temperature is detected either in the DDM-correlated noise maps, but residual levels of DDM-correlated noise tend to coincide with coastal regions and other densely populated areas (e.g., Western Europe). Overall, ambient noise levels are significantly lower over polar regions than over land, both for MBD- and DDM-correlated noise, lending support to the idea that ambient noise is linked to the level of human activity.

Figs. 13 and 14 present the same data as in Fig. 12 but split into individual descending (top, day-time) and ascending (bottom, night-time) tracks, for DDM-correlated noise power and MBD, respectively. These plots confirm that high L1 ambient noise in the hotspots regions is observed in both ascending and descending tracks, and in both MBD- and DDM-correlated noise. There are marked differences in the spatial distribution of the hotspots between ascending and descending tracks, indicating a dependence on the FOV of the antenna, which differs for ascending and descending tracks due to the backward pointing of the antenna and the anisotropy of the antenna radiation pattern. The MBD maps in Fig. 14 suggest a strong diurnal signature in ambient noise levels, with land generally appearing brighter during daytime (descending tracks, Fig. 14 top) than during the night (ascending tracks, Fig. 14 bottom), which confirm a relation with the generally higher levels of human activity in daytime.

The slight meridional displacement of the hotspots in ascending and descending passes lends support to the hypothesis that the elevated noise in these regions is linked to surface reflections of GNSS L1 signals transmitted by other GNSS satellites. Thus, in addition to emissions from other GPS transmitters, there are signals originating also from constellations in geostationary orbit, such as the SBAS, which currently consists of several geostationary satellites in the equatorial plane at longitudes close to those observed hotspots, and the quasi-zenith satellite system (QZSS), which currently has a single satellite (Michibiki) that describes a highly elliptical geosynchronous figure-of-8 ground track over Western Pacific to deliver improved positioning capability to Japan. Similarly, the Beidou satellite navigation system comprises not only MEO-inclined orbiting satellites similarly to GPS, but also geostationary and inclined geosynchronous orbits. With the presence of Beidou and QZSS inclined geosynchronous satellites over Asia, a diurnal variation in signal reflection between Northern and Southern hemispheres might be expected. Such a diurnal variation is visible in Figs. 13 and 14, between the China Sea in the descending pass and Indian Ocean in the ascending pass. Overall, the hotspots are likely to originate from a multitude of GNSS sources although more detailed investigations would be required to confirm attribution to specific satellites.

It is notable that typically higher noise is observed over the ocean compared to land, pointing to a link to the stronger reflecting properties of the ocean at L-band compared to land surfaces. Both the correlated noise power and the MBD uncorrelated noise feature L1 GNSS radiation reflected into the FOV

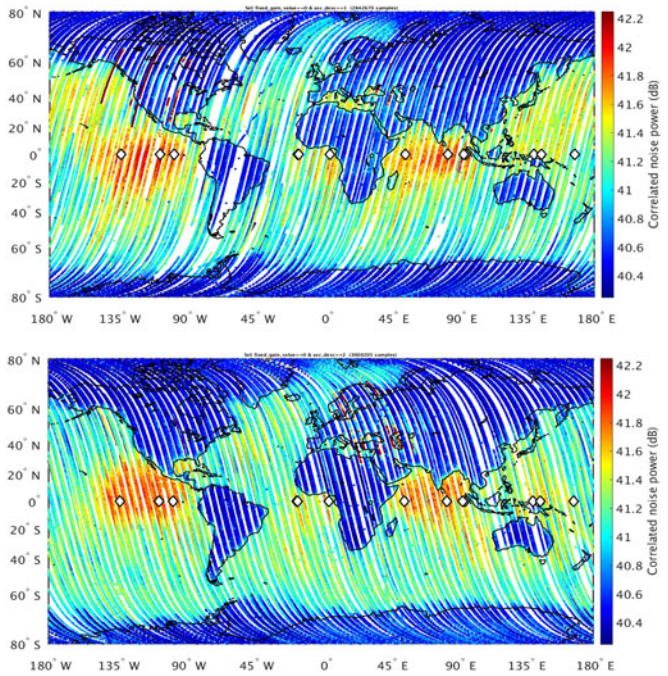

Fig. 15. TDS-1 DDM-correlated noise power (N) for uncalibrated data acquired in automatic gain mode (AGM) between May 2015 and February 2016 for (top) descending tracks and (bottom) ascending tracks. White lozenges as in Fig. 12.

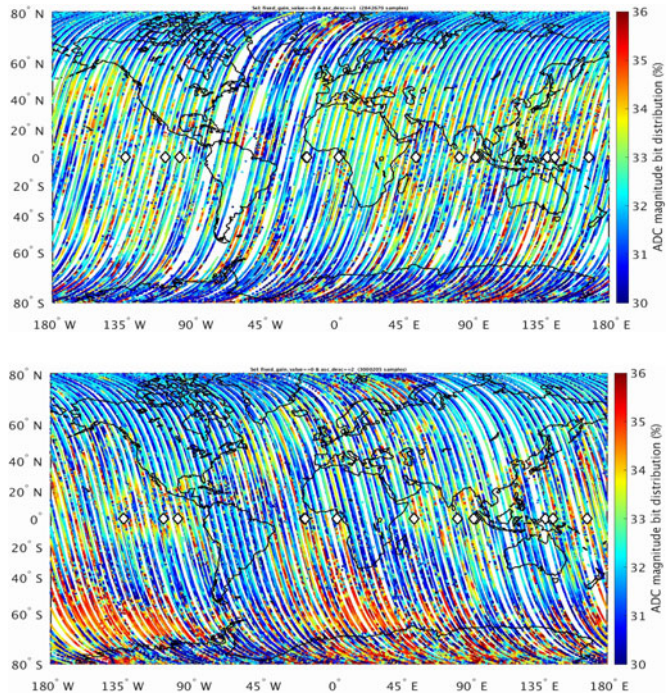

Fig. 16. TDS-1 magnitude bit distribution (MBD) for uncalibrated data acquired in automatic gain mode (AGM) between May 2015 and February 2016 for (top) descending tracks and (bottom) ascending tracks. White lozenges as in Fig. 12.

of the antenna, with these contributions being particularly strong when reflections occur over the ocean.

2) Observed L1 Ambient Noise in AGM: Figs. 15 and 16 present similar maps as in Figs. 13 and 14 but for uncalibrated TDS-1 data acquired in automatic gain mode between May 2015 and February 2016. The DDM-correlated noise (see Fig. 15) and the MBD (see Fig. 16) are shown separately for individual descending (top) and ascending tracks (bottom).

In AGM, the global mean MBD is 32.3% and well constrained for both descending and ascending tracks within a range of ∼6%. The mean MBD is close to the optimal level corresponding to minimum implementation loss (33%) and is consistent with the expected behavior of the AGC. The range of the MBD is slightly narrower for AGM (6%) than for PGM (12%), confirming that although the AGM performs better than PGM with regards to minimizing implementation losses, it does not perfectly maintain the optimal level. This may be due to the 1 dB granularity of the gain control.

Contrary to what was seen for PGM, the DDM-correlated noise and the MBD differ significantly from each other when data are acquired in AGM. The MBD obtained in AGM gives a random appearance, with no sharp land/ocean contrasts and no spatially coherent patterns in the equatorial hotspots regions (although the edges of the hotspots are discernible in places). This is consistent with the operation of the AGC, which adjusts the system gain to accommodate large changes in incoming radiation levels, and through its action, obscures the underlying ambient noise variations seen in Figs. 13 and 14.

The sharp transitions visible between 36% and 30%, for example, in the South Pacific of the MBD ascending tracks in Fig. 13 are likely to be due to the threshold being crossed causing a 1 dB change in gain to be automatically applied. In contrast, the DDM-correlated noise shows similar patterns in AGM as in PGM, with clearly defined noise hotspots along the Equator, albeit weaker in magnitude. This indicates that, even in AGM, the DDM-correlated noise levels reveal non-negligible contributions by other L1 GNSS sources, most likely after reflection off the ocean surface into the TDS-1 antenna field of view.

IV. Discussion

We presented an overview of the TDS-1 GNSS-R dataset acquired to date in various instrumental modes, highlighting a number of non-geophysical factors in spaceborne GNSS-R that could impact the geophysical inversion and interpretation of GNSS-R signals typically used for the retrieval of winds and ocean roughness.

A. Eclipse and Attitude

Analyses included an assessment of the quality of TDS-1 platform-related information provided in new products released on MERRByS since May 2016, featuring a revised eclipse flag and the attitude estimation data recorded by the onboard attitude determination system. It was confirmed that the new eclipse flag in v0.5 offers a more reliable handle for data quality control than in earlier MERRByS products, performing as expected with only occasional anomalies that still remain under investigation.

The attitude estimate data from the onboard attitude determination system indicated that the magnitude of attitude

adjustments in eclipse is small, but this was shown to give a false sense of confidence in the stability of the platform while in eclipse. Indeed, large attitude corrections of the order of 10° observed when the satellite emerges from eclipse (over high-latitudes or polar regions) indicate that the platform drifts significantly while in eclipse, and that attitude uncertainty while in eclipse remains no better than 10°. TDS-1 attitude in sunlit parts of the orbit is found to be generally better, with attitude estimate typically smaller than 1°, except for very large attitude fluctuations of up to 10° observed in several zonal bands at mid-latitudes in both hemispheres. Fortunately, these large attitude corrections affect only a small proportion of data acquired in sunlit passes, with over 95% of data associated with attitude adjustments smaller than 1.5°.

Even so, the impact of attitude uncertainty on TDS-1 data turns out to be nontrivial and needs more complex considerations than simple application of an eclipse flag. The impact will greatly depend on the location of SP in the antenna gain map, with SP outside the –6 dB edge of the main lobe—which represents a substantial proportion of reflections collected by TDS-1—subject to the largest uncertainty in the determination of the AGSP. The TDS-1 platform attitude uncertainty represents an important limitation of the TDS-1 GNSS-R dataset, introducing multiple layers of complexity that make it difficult to confidently establish the dependence of GNSS-R signals on secondary geophysical effects.

B. L1 Ambient Noise in PGM and AGM

TDS-1 data were analyzed to examine L1 ambient noise levels as revealed by DDM-correlated noise levels and MBD. The noise levels found in the L1 band here, within the bandwidth of the receiver (a couple of MHz), are not necessarily representative of those that might be found across the whole of the L-band (which is much broader). Analyses were performed for TDS-1 SGR-ReSI data acquired in PGM and AGM. Given the uncalibrated nature of the data presented here, further investigation awaits the use of the calibrated data that have only recently become available from TDS-1.

Several well-defined L1 noise hotspots were revealed along the Equator and in the Western Pacific thought to be related to reflected signals from GNSS satellites including some in geostationary orbits. L1 ambient noise levels are generally higher over ocean than over land and ice, possibly linked to the higher reflectivity of the ocean leading to stronger contributions by other L1 radiation reflected into the TDS-1 nadir antenna FOV.

The Equatorial noise hotspots are observed in the DDM-correlated noise levels for both PGM and AGM, albeit with smaller magnitude in AGM. Nevertheless, these strong permanent noise sources will impact DDM observables used for geophysical inversion such as the SNR, potentially leading to incorrect inferences about links to geophysical ocean properties such as near-surface wind, sea surface temperature, or salinity. Techniques based on the DDM SMN would be less sensitive to RF contamination compared to equivalent DDM SNR estimates, although the lack of knowledge of system gain in AGM means that the use of DDM SMN would remain limited to data acquired in PGM, provided that system gain and noise figure (which both depend on on-board temperature that could change due to orbital drift) are sufficiently stable. Ultimately, radiometric calibration should be used whenever possible to mitigate these effects, together with proper characterization of the direct signals.

The MBD provides some evidence of sensitivity of L1 ambient noise to human activity levels that is most noticeable from the large diurnal change in noise levels over populated regions and from low noise levels in unpopulated land and ice regions (e.g., central Australia, Antarctica). Elsewhere, high-power L1 radiation levels are sporadically observed in certain regions, indicating a human origin, and the persistence of some sources in DDM-correlated noise estimates suggests the presence of GNSS-related signals. The impact of RFI on GNSS-R is already well documented [14], [15] and strategies for the detection and mitigation of these transitory high-power RFI events are currently under investigation.

V. Conclusion

Spaceborne GNSS-R data from the UK TDS-1 mission were examined to report on key features of the TDS-1 dataset and highlighting various non-geophysical effects in the data. The assessment was motivated by the need to understand the qualities and limitations of the TDS-1 dataset, which—as the first comprehensive globally distributed set of spaceborne GNSS-R data—are currently used extensively by the scientific community to ascertain the sensitivity of GNSS-R signals to Earth surface properties.

Our assessment indicates that earlier reliability issues with the eclipse flag in the TDS-1 products have been mostly addressed in L1 products released via MERRByS since May 2016. The products now also include new information about platform attitude estimates that give indirect indications about platform attitude error in eclipsed and non-eclipsed parts of the orbit. It confirms that attitude errors are likely to grow to the order of 10° in eclipse. Out of eclipse, the attitude estimate typically remains smaller than 1.5° although large attitude adjustments of up to 10° are occasionally observed in sun-lit part of the orbits for reasons that remain unclear. These large attitude adjustments occur in two well-defined narrow bands at midlatitudes in the Northern and Southern hemispheres, but affect less than 5% of the overall sun-lit data. These uncertainties in platform attitude represent an important limitation of the TDS-1 GNSS-R dataset, particularly since most SPs occur outside the half-power beam of the nadir antenna where even small attitude errors can lead to large errors in the AGSP and inaccurate geophysical interpretation of the signal power level. Further work is ongoing on the TDS-1 satellite platform to address the attitude determination limitations, and in particular, new complementary attitude measurements may become available from the three zenith antennas that the SGR-ReSI supports.

Finally, global maps were presented of the L1 ambient noise as sensed by the TDS-1 SGR-ReSI instrument, revealing several persistent hotspots along the Equator that are most likely associated with surface reflections from GNSS satellites.

Sporadic high-power noise events observed certain regions point to sources of human origin. Differences in L1 noise level seen in the DDM noise and the MBD provide further information about the correlated and uncorrelated nature of the L1 noise source. Elsewhere, noise levels differ markedly for GNSS-R data collected over ocean, ice, and land surfaces. Noise levels are particularly elevated for reflections from the ocean, indicating that the effect is closely related to the scattering properties of the surface. Before correlation, L1 ambient noise in the MBD maps shows a strong relation with human activity levels, as confirmed by low noise levels in regions of low human activities (deserts, polar regions). After correlation, the link between DDM-correlated noise and human activity level is no longer readily detectable except for residual signatures in very densely populated regions (e.g., coastal zone).

This work has shown that while operation in AGM may offer a good method for cancelling instrument gain from both the signal and noise, it masks the variation of the underlying noise floor. This noise is shown to change by as much as 2.5 dB, and so will add an error in the estimation of the reflected signal power by the same amount if using an SNR-based observable.

When operating in PGM, the underlying noise is not masked, and can be measured. The drawback of using a signal minus noise observable is that the instrument gain is no longer cancelled and so a known power is required to which the noise measurement may be referenced for calibration. An important conclusion of this study is that care should be taken when considering using noise measurements over the equatorial oceans for calibration purposes, as there is more variation than might be expected. There are more consistent regions of the globe that make better targets, for example, South America and the poles appear to be relatively consistent and clear of interference.

The SGR-ReSI is equipped with switched "black-body" loads to give an internal reference measurement. Work is ongoing with these switched loads and together with the attitude improvements, TDS-1 will continue to support the understanding and validation for GNSS-R for remote sensing in the future.

ACKNOWLEDGMENT

The authors are grateful for the helpful comments by two anonymous reviewers.

REFERENCES

[1] M. Unwin *et al.*, "Development of low-cost spaceborne multi-frequency GNSS receiver for navigation and GNSS remote sensing," *Int. J. Space Sci. Eng.*, vol. 1, pp. 20–50, 2013.

[2] C. Ruf *et al.*, "CYGNSS: Enabling the future of hurricane prediction [remote sensing satellites]," *IEEE Geosci. Remote Sens. Mag.*, vol. 1, no. 2, pp. 52–67, Jun. 2013.

[3] H. Carreno-Luengo *et al.*, "3Cat-2-an experimental nanosatellite for GNSS-R earth observation: Mission concept and analysis," *IEEE J. Sel. Topics Appl. Earth Obs. Remote Sens.*, vol. 9, no. 10, pp. 4540–4551, Oct. 2016.

[4] G. Foti *et al.*, "Spaceborne GNSS-reflectometry for ocean winds: first results from the UK TechDemoSat-1 mission," *Geophys. Res. Lett.*, vol. 42, pp. 5435–5441, 2015. Doi: 10.1002/2015GL064204.

[5] P. Jales and M. Unwin, "TechDemoSat-1 mission description," Surrey Satell. Technol. Ltd., Surrey, U.K., 2016. [Online]. Available: http://www.merrbys.co.uk.

[6] M. Unwin, P. Jales, J. Tye, C. Gommenginger, G. Foti, and J. Rosello, "Spaceborne GNSS-reflectometry on TechDemoSat-1: Early mission operations and exploitation," *IEEE J. Sel. Topics Appl. Earth Obs. Remote Sens.*, vol. 9, no. 10, pp. 4525–4539, Oct. 2016.

[7] C. S. Ruf *et al.*, "New ocean winds satellite mission to probe hurricanes and tropical convection," *Bull. Amer. Meteorol. Soc.*, vol. 97, pp. 385–395, 2016.

[8] M. P. Clarizia, C. S. Ruf, P. Jales, and C. P. Gommenginger, "Spaceborne GNSS-R minimum variance wind speed estimator," *IEEE Trans. Geosci. Remote Sens.*, vol. 52, no. 11, pp. 6829–6843, Nov. 2014. Doi: 10.1109/TGRS.2014.2303831.

[9] P. Misra and P. Enge, *Global Positioning System: Signals, Measurements and Performance*. 2nd ed. Lincoln, MA, USA: Ganga-Jamuna Press, 2006.

[10] V. U. Zavorotny and A. G. Voronovich, "Scattering of GPS signals from the ocean with wind remote sensing application," *IEEE Trans. Geosci. Remote Sens.*, vol. 38, no. 2, pp. 951–964, Mar. 2000.

[11] S. Gleason and D. Gebre-Egziabher, *GNSS Applications and Methods*. Norwood, MA, USA: Artech House, 2009.

[12] J. B. Hagen and D. T. Farley, "Digital correlation techniques in radio science," *Radio Sci.*, vol. 8, pp. 775–784, 1973.

[13] X. Bosch-Lluis, I. Ramos-Perez, A. Camps, N. Rodriguez-Alvarez, E. Valencia, and H. Park, "A general analysis of the impact of digitization in microwave correlation radiometers," *Sensors*, vol. 11, pp. 6066–6087, 2011.

[14] R. Onrubia, J. Querol, D. Pascual, A. Alonso-Arroyo, H. Park, and A. Camps, "DME/TACAN impact analysis on GNSS reflectometry," *IEEE J. Sel. Topics Appl. Earth Obs. Remote Sens.*, vol. 9, no. 10, pp. 4611–4620, Oct. 2016.

[15] J. Querol, A. Alonso-Arroyo, R. Onrubia, D. Pascual, H. Park, and A. Camps, "SNR degradation in GNSS-R measurements under the effects of radio-frequency interference," *IEEE J. Sel. Topics Appl. Earth Obs. Remote Sens.*, vol. 9, no. 10, pp. 4865–4877, Oct. 2015.

Giuseppe Foti received the M.Eng. degree in electronics engineering from the University of Catania, Catania, Italy, in 2000, and the M.Sc. degree in oceanography from the University of Southampton, Southampton, U.K., in 2013.

In 2001, he joined the Communication Systems Section of the European Space Agency, Noordwijk, The Netherlands, where he conducted research in the field of spread-spectrum techniques for packet access in broadband satellite systems. From 2003 to 2010, he served at the European Patent Office, Rijswijk, The Netherlands, as Patent Examiner in the Principal Directorate of Telecommunications. In 2013, he joined the Satellite Oceanography Section of the National Oceanography Centre, Southampton, U.K., where he currently works as Research Scientist. At present, his research interests focus on remote sensing of the oceans, with special emphasis on techniques using signals of opportunity.

Christine Gommenginger received the Diplome d'Etudes Approfondies in electromagnetics, telecommunications and remote sensing from the University of Toulon, La Garde, France-University of Nice Sophia Antipolis, Nice, France, and the Ph.D. degree from the University of Southampton, Southampton, U.K., in microwave radar remote sensing of the ocean at low grazing angles.

She has worked with the National Oceanography Centre, Southampton, U.K., for more than 20 years. Her research interests include active and passive microwave remote sensing of the ocean, understanding interactions of microwave signals with the ocean surface, remote sensing of ocean wind and waves, and developing new Earth observation technologies and applications. Her work includes research in altimetry for sea state, along-track interferometric synthetic aperture radar (SAR) for currents, global navigation satellite system reflectometry for surface winds and sea state, SAR altimetry, salinity from space with soil moisture ocean salinity, and wide-swath ocean altimetry.

Martin Unwin worked toward the Ph.D. degree in spaceborne GPS from 1991 to 1995 at the University of Surrey, Surrey, U.K.

He initiated and led the GPS team in Surrey Satellite Technology Limited (SSTL), Surrey, U.K., designing the SGR-20 space GPS receiver which flew on UoSAT-12 and Proba-1. The GPS team succeeded in demonstrating autonomous orbit control, attitude determination in orbit, operation of GPS above the GPS constellation, and the feasibility of GPS reflectometry on the UK-disaster monitoring constellation satellite. He has had involvement in GIOVE-A and Galileo FOC projects from the beginning. He is currently a Principal Engineer in SSTL and is working on the development of the SGR-Axio receiver, the SGR-ReSI exploitation on TechDemoSat-1, and the NASA CYGNSS mission.

Dr. Unwin received the Institute of Navigation Tycho Brahe Award 2011, and the GPS World Leadership award, 2012.

Philip Jales received the M.Phys. degree in physics from the University of Manchester, Manchester, U.K., in 2007, and the Ph.D. degree from the University of Surrey, Surrey, U.K., in 2012, in GNSS-reflectometry techniques, specializing in new receiver approaches.

He is currently a Senior Engineer with Surrey Satellite Technology Limited (SSTL), Surrey, U.K., working on the reflectometry-capable space global navigation satellite system receivers, the SGR-ReSI, and SGR-Axio. He is supporting both the NASA CYGNSS mission and the TechDemoSat-1 reflectometry exploitation experiment.

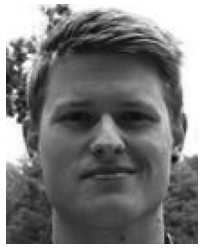

Jason Tye received the M.Sc. degree in theoretical physics from the University of Birmingham, Birmingham, U.K., in 2013. Since then he has been working toward the Ph.D. degree in developing the applications of spaceborne GNSS-R, utilizing data from SSTL's SGR-ReSI on TechDemoSat-1.

His research interests include understanding receiver effects on delay–Doppler maps and novel methods of wave and ice sensing.

Josep Roselló received the Graduate degree as a Telecommunications Engineer in 1991 from the Politechnical University of Catalonia, Barcelona, Spain.

He started working in 1993 with the European Space Research and Technology Centre (ESTEC) Technical Directorate, Noordwijk, The Netherlands, in signal and data processing of Earth observation and Galileo payloads. Since 2007, he has been in the Future Missions Division of the Earth Observation Directorate, ESTEC. His current responsibilities include internal research and technical management of industrial and academic contracts, as well as interagency co-ordination. He is leading in European Space Agency the deployment from low Earth orbit of the data downlink in the 25.5–27 GHz k-band and the development of new global navigation satellite system payloads for Earth observation.